Supramolecular Chemistry
Publication details, including instructions for authors and subscription information:
http://www.informaworld.com/smpp/title~content=t713649759

Ion pair binding functionalised gold nanoparticles

Maria H. Filby[a]; Jonathan W. Steed[a]
[a] Department of Chemistry, Durham University, Durham, UK

To cite this Article Filby, Maria H. and Steed, Jonathan W.(2009) 'Ion pair binding functionalised gold nanoparticles', Supramolecular Chemistry, 21: 5, 422 — 427
To link to this Article: DOI: 10.1080/10610270802165951
URL: http://dx.doi.org/10.1080/10610270802165951

Supramolecular Chemistry
Vol. 21, No. 5, July–August 2009, 422–427

Taylor & Francis
Taylor & Francis Group

Ion pair binding functionalised gold nanoparticles

Maria H. Filby and Jonathan W. Steed*

Department of Chemistry, Durham University, Durham, UK

(*Received 7 March 2008; final version received 23 April 2008*)

Pyridyl amide functionalised gold nanoparticles have been used to bind and sense simple anions and ion pairs by means of shifts in the intensity and wavelength of the nanoparticles' surface plasmon resonance absorption.

Keywords: gold nanoparticles; anion; ion pair; sensing; amide; supramolecular

Introduction

In recent years, there have been several studies aimed at attaching supramolecular anion recognition functionality to the surface of metallic nanoparticles, particularly gold (*1–3*). Nanoparticle attachment allows the coupling of selective binding functionality with the photophysical properties of the nanoparticle, namely the surface plasmon absorption band (*4*). Moreover, binding to nanoparticles can serve to enhance the preorganisation of the receptor functionality by rigidifying and preorganising the binding pocket (*1*). Thus functionalisation of gold nanoparticles with ion recognition functionality provides an interesting potential ion sensing paradigm.

Recently, we have shown that simple hydrogen bonding pyridyl ligands (*5–7*) are capable of self-assembling with particular anion–metal combinations. This process results in discrete arrays held together by co-operative hydrogen bonding of anions such as NO_3^- between pairs of ligands, coupled with simultaneous binding of the pyridyl functionality to the metal centre (*6*, *7*) and this recognition motif can form the basis of a series of pyridinium anion-binding hosts (*8–13*) and can be transferred to a polystyrene support (*14*). This work forms part of a growing body of interest in metal-based anion receptors (*15–19*). We now report the coupling of a self-assembled, labile ion pair binding system to gold nanoparticles.

Ligands **1** and **2** were designed to incorporate a cation-ligating pyridyl group, an anion-binding amide and a disulphide or dithiol moiety capable of binding strongly to a gold nanoparticle surface. We anticipate a simultaneous anion- and cation-binding mode, as shown in Figure 1. Beer et al. (*1*) have reported simple thioctic acid amide derivatives capable of binding anions with association constants in the region of $10^5\,M^{-1}$ and we anticipate an additional enhancement from the preorganisation imparted by attachment to the nanoparticle. Ligand **1** is readily synthesised by coupling of thioctic acid and 3-aminopyridine with DCCI (3-dimethylaminopropyl)-ethyl-carbodiimide (EDC) and hydroxybenzotriazole hydrate (HOBt) in dichloromethane.

Gold nanoparticles were prepared by a literature method (*20*). The reduced gold was exposed to air after being stirred for 10 min to quench any remaining reducing agent. Ligand **1** was then added (two equivalents based on $HAuCl_4$) and the mixture stirred for a further hour. The functionalised nanoparticles (**3**) (Figure 2) precipitate readily from diethylene glycol dimethyl ether (diglyme) solution and were purified by ultracentrifugation and several washings with diethyl ether to remove any unreacted ligand, naphthalene and diglyme. The nanoparticles were then redissolved in methanol. Transmission electron microscopy (TEM) images confirm the presence of nanoparticles with sizes varying between *ca.* 4 and 9 nm. The presence of the organic ligand was confirmed by thermogravimetric analysis (TGA) analysis, which showed *ca.* 20% mass loss in the range 170–400°C. The nanoparticles remained stable and did not agglomerate in solution at room temperature over a period of 6 months. The solvent can be removed and the nanoparticles can be redispersed in a variety of solvents. Binding of the ligand to the nanoparticles was confirmed in this way by the observation of broadened ligand signals (*21*) in the ^{1}H NMR spectrum of the functionalised nanoparticles in methanol-d_4 (see Figure S1). The ^{1}H NMR spectroscopic resonances are characteristically broadened relative to those of free ligand because of spin–spin relaxational (T_2) broadening, differences in Au-SR binding sites and a gradient in monolayer packing density from near core to ligand terminus with associated dipolar broadening. The IR spectra of ligands **1** and **2** and the functionalised nanoparticles (**3**) were recorded as KBr discs. Peaks observed at 634 and 706 cm^{-1} were assigned to S—S and C—S stretching modes, respectively, both of which disappear

*Corresponding author. Email: jon.steed@durham.ac.uk

ISSN 1061-0278 print/ISSN 1029-0478 online

DOI: 10.1080/10610270802165951
http://www.informaworld.com

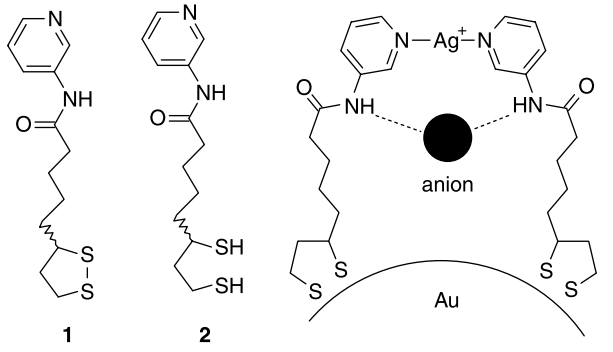

Figure 1. Structures of ligands **1** and **2** along with the proposed binding mode of the ligand–salt complex to the nanoparticle surface.

upon adsorption onto the gold surface. While nanoparticles derived from ligands **1** and **2** were broadly similar, those derived from the disulphide **1** proved to exhibit better long-term stability, and as a result we focused on this compound.

The UV–vis spectrum of the functionalised nanoparticles **3** in methanol solution showed a broad peak at 531 nm, assigned to the nanoparticle surface plasmon resonance (SPR) band. The measurement was repeated 1 week later without any sign of aggregation or ageing (*22*). The anion- and cation-binding ability of the functionalised nanoparticles was assessed by titration with potential guest species. In a typical experiment, 10 μl aliquots of guest solution (0.216 mol dm^{-3}) were added to a 2 ml sample of the gold nanoparticle solution.

Figure 3 reveals a small red shift from 532 to 535 nm, which occurs upon addition of up to six aliquots of Cl^-. Then, on each further addition, a much larger change is observable and the absorption maximum reaches 553 nm after an addition of a total of 0.1 ml of the anion solution. The change is ascribed to anion binding to the amide hydrogen bonding moiety of the ligand and consequent changes in the local index of refraction followed by nanoparticle cross-linking. Dialysis of the solution to remove excess $NBu_4^+Cl^-$ did not result in any change in the absorption suggesting that binding is irreversible under the experimental conditions. By contrast, analogous titration with Br^- resulted in no significant changes other than dilution effects (see supplementary data), indicating much weaker binding of the bromide anion. Titration with NO_3^- resulted in a similar change to that observed for chloride; however, the binding appeared weaker as the shift had reached 550 nm only after an addition of 0.2 ml in total (see supplementary data). In the case of Cl^-, Br^- and NO_3^-, there was a decrease in absorbance due to dilution effects. When the nanoparticle solution was titrated with $MeCO_2^-$ in the same way, however, an initial increase in absorbance and a red shift were observed after the addition of up to three aliquots of anion solution followed by a decrease in absorbance and a further red shift, reaching 556 nm after an addition of only eight aliquots (see Figure S7). The reason for the increase in absorbance is unclear, although it is possible that the subsequent decrease and red shift is due to excess acetate ions bridging between nanoparticles causing aggregation.

Since the functionalised nanoparticles appear to exhibit anion-binding effects, we turned our attention to cation binding, in particular using Ag(I), which is likely to interact strongly with the pyridyl groups as we have observed in related systems in solution (*7*). Titration of nanoparticles **3** with $AgBF_4$ proved interesting, with a significant increase in the absorption in proportion with the amount of added Ag^+ until a limiting spectrum was reached after the addition of four aliquots, at which point further addition resulted in a decrease in the absorption and a red shift (Figure 4). It has been shown (*23*) that nanoparticle surface plasmon

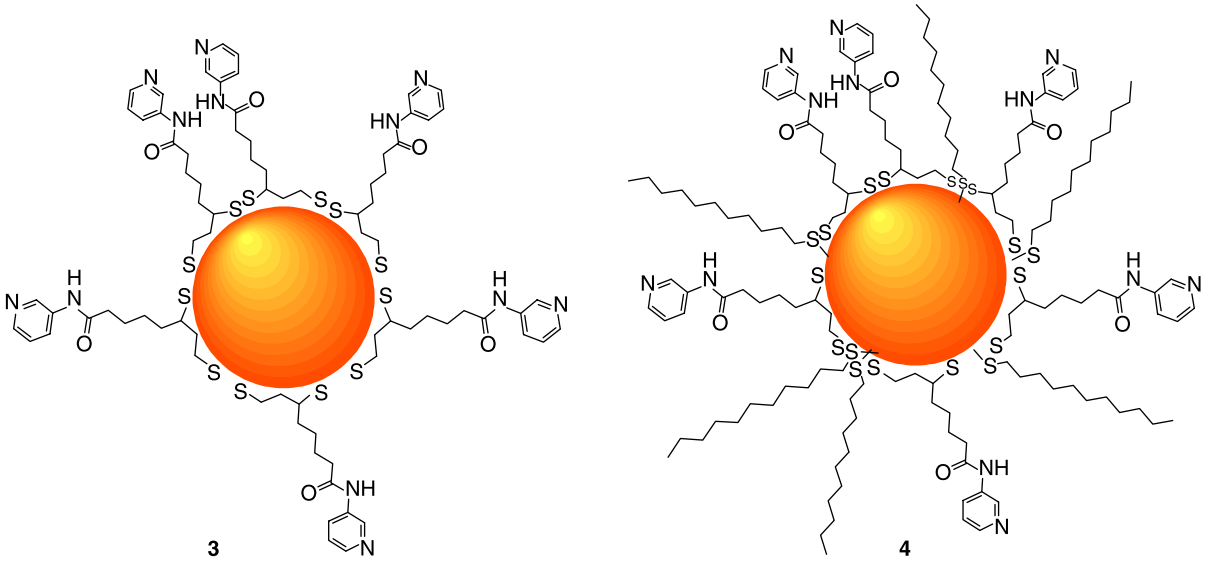

Figure 2. Schematics of functionalised gold nanoparticles **3** and **4**.

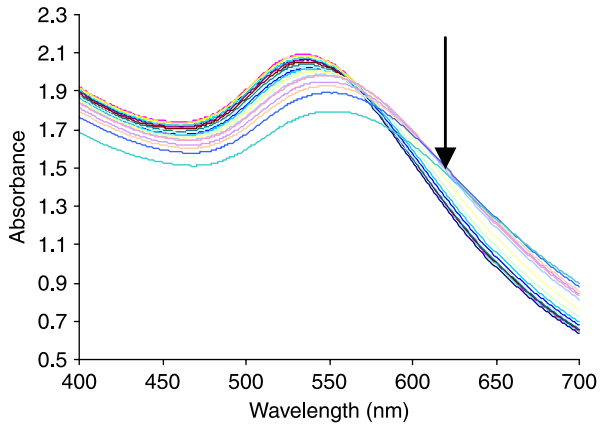

Figure 3. Titration of gold nanoparticles **3** with NBu_4Cl in methanol. The uppermost spectrum is the pure nanoparticle solution.

absorption intensity increases with increasing thickness of a surrounding silica shell, although relatively thick (10 nm) shells are required. This observation is explained by an increase in the significance of scattering. It is difficult to see how such a dielectric layer could form in this instance, however. An alternative explanation may be binding of Ag(I) to the surface of the nanoparticle itself resulting in a size increase and hence increase in absorption coefficient, although in this case a shift to longer wavelength would also be expected. When the layer deposition is saturated, the excess silver tetrafluoroborate may cause the gold nanoparticles to aggregate and eventually precipitate out of solution to give a final red shift and decrease in absorbance in the final spectrum.

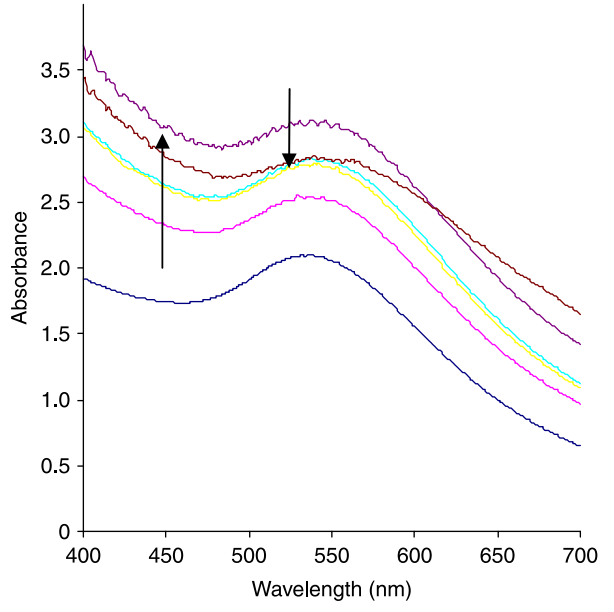

Figure 4. Titration of gold nanoparticles **3** solution with $AgBF_4$ in methanol. The bottom spectrum is the pure nanoparticle solution.

Further, interesting results were observed upon titration of functionalised nanoparticles **3** with $AgNO_3$ solution. In related small molecule model systems, we have shown a significant co-operativity between Ag^+ and NO_3^- binding (*7*). Upon addition of $AgNO_3$ to a solution of **3** in methanol, initially a significant increase in absorbance was observed, accompanied by a red shift from 535 to 550 nm; on addition of a further aliquot of $AgNO_3$, however, the absorbance rapidly decreased, accompanied by significant broadening, attributed to agglomeration and eventual precipitation of the nanoparticles. This behaviour may be correlated with the initial formation of discrete assemblies followed by more open species upon addition of excess nitrate in the small molecule systems. Thus, we speculate that the formation of a shell of bound ion pairs, the type shown in Figure 1, might result in increased absorption, followed by agglomeration as Ag^+ and NO_3^- anions begin to cause cross-linking between nanoparticles (*24*, *25*).

As a control, we also examined dodecanethiol-protected nanoparticles that lack ion-binding functionality (*26*). The nanoparticles were subjected to several UV–vis titrations with anions in chloroform in the same way as **3** (the much more lipophilic dodecane thiolate-protected nanoparticles are not soluble in methanol). There was no spectral change in any of the titrations with anions or Ag^+ other than a decrease in absorbance due to dilution effects. An attempt was also made at synthesising ligand **1**-protected nanoparticles using the Schiffrin method (*27*). However, the nanoparticles precipitated within a course of several hours probably due to the formation of larger aggregates that hydrogen bond the ligand to an excess of bromide, an event that is more likely to occur in low polarity solvent such as chloroform.

We also examined a ligand exchange procedure to prepare mixed dodecanethiol/**1**-protected nanoparticles (*1*, *2*). One molar equivalent of ligand **1** to $HAuCl_4$ was added to the dodecanethiol-protected nanoparticles, followed by stirring for 24 h. The nanoparticles were then precipitated with methanol, centrifuged and washed. The nanoparticles were redissolved in chloroform and the resulting mixed nanoparticles (**4**) were characterised by ^{1}H NMR spectroscopy, IR and TEM. The ^{1}H NMR spectrum reveals the ratio of dodecanethiol to ligand as 1.7:1 by integration. Broadening of the peaks is also noted, however, not to such extent as it was seen in the pure ligand nanoparticles. This could be attributed to more regular size of the nanoparticles and slightly smaller diameter (*28*). The binding properties of the mixed monolayer-protected nanoparticles **4** were also probed with UV–vis titration in chloroform solution. There was only an observable change in SPR shift upon addition of chloride anion. Interestingly, the first addition produced larger red shift than in pure ligand nanoparticle solution (**3**). This is most likely due to the solvent used, which is of lower polarity promoting stronger hydrogen bonding. Subsequent

additions produced further red shift until the SPR absorption reached 535 nm after which point the SPR band returned to almost its original position at 530 nm. This behaviour could be attributed to the mobility of the ligands around on the surface of the nanoparticle or insufficient density of ligand **1** on the nanoparticle surface to give co-operative binding.

The TEM images of nanoparticles **4** reveal much higher monodispersity than **3** with nanoparticles and average diameters of around 5 nm. The mixed nanoparticles (**4**) appear to be more agglomerated in comparison with pure dodecanethiol-protected nanoparticles (Figure 5).

Finally, we also attempted to exchange citrate-stabilised commercial gold nanoparticles of an average diameter of 8–12 nm with ligand **1**. The absorption wavelength of the citrate-stabilised nanoparticles occurs at 524 nm. Addition of small aliquots of methanolic solutions of various concentrations of **1** resulted in a profound red shift of the absorption wavelength (depending on concentration) and finally the nanoparticles precipitated out irreversibly. This behaviour could be due to the ligand adsorbing onto the surface of gold and then binding the citrate anions still present in solution, which could subsequently lead to the formation of larger aggregates via hydrogen bonding interactions.

In conclusion, we have shown that gold nanoparticles functionalised with simultaneous anion- and metal-binding ligands can exhibit mixed effects according to the ability of the anions to either bind to or cross-link nanoparticles. Silver(I) binding results in enhanced absorbance and simultaneous silver(I) and nitrate binding results in a co-operative effect, in which enhanced absorption is observed in the presence of small amounts of $AgNO_3$ but switching to agglomeration behaviour upon addition of excess metal salt.

Experimental section

All purchased starting materials were of commercial quality and used without further purification. Solvents were used as obtained, unless mentioned otherwise. Dichloromethane was dried using a calcium hydride still. Diglyme was dried over sodium under vacuum. Reactions were carried out under air unless specifically mentioned. ^{1}H NMR spectra were run at room temperature using Bruker AV400, Varian Inova500, Varian Unity-300 and Varian Mercury-200 NMR spectrometers at the Durham University. Chemical shifts are reported in parts per million (δ) relative to tetramethylsilane as an internal standard. Mass spectra were run using Micromass Autospec operating in EI or ES mode at the Durham University. Micro-analysis for C, H and N were recorded at the Durham University. IR spectra were collected using Perkin-Elmer Spectrum 100 (spectral resolution 4 cm^{-1}) as KBr discs. UV spectra were recorded on Perkin-Elmer Lambda 900 UV/VIS/NIR spectrometer.

5-[1,2]Dithiolan-3-yl-pentanoic acid pyridin-3-ylamide (1)

Thioctic acid (0.825 g, 4.0 mmol) and EDC (0.621 g, 4.0 mmol) were dissolved in dichloromethane (70 ml) and stirred for 2 h. Hydroxybenzotriazole hydrate (HOBt) (0.540 g, 4 mmol) was added followed by 3-aminopyridine

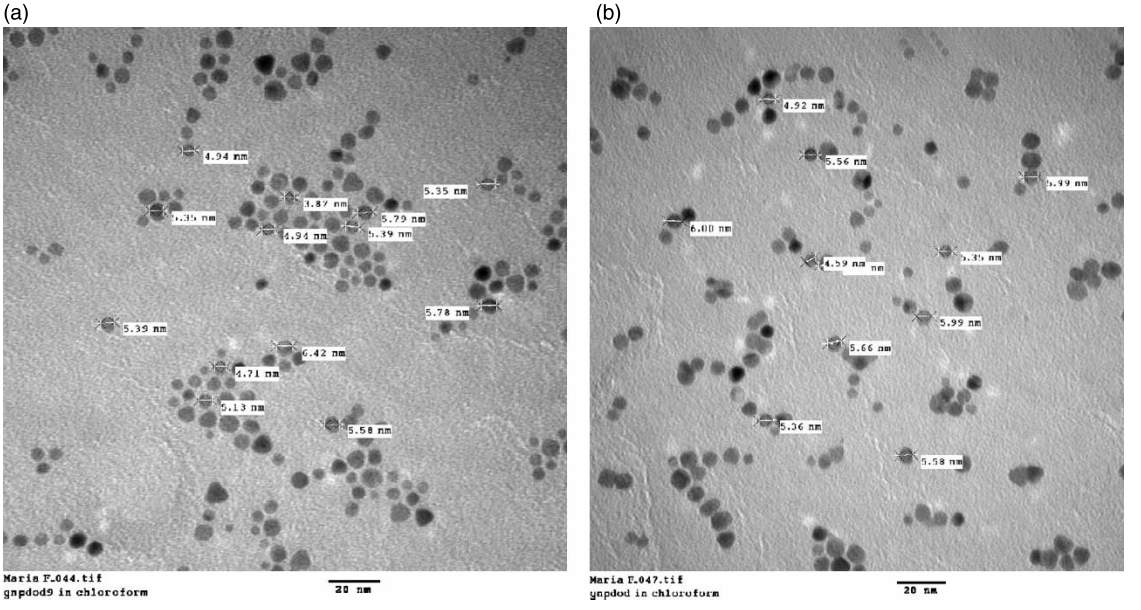

Figure 5. TEM images of mixed layer (dodecanethiol/ligand) functionalised nanoparticles **4** (a) and pure dodecanethiol-protected nanoparticles (b).

(0.37 g, 4 mmol). The reaction mixture was stirred at room temperature for 24 h. The solvent was then removed under vacuum and the resultant oil was washed several times with water until pure. ^{1}H NMR ($CDCl_3$, J (Hz), δ (ppm)): 1.38–1.44 (m, 2H, CH_2), 1.48–1.68 (m, 4H, CH_2), 1.81–1.83 (q, $J = 6.8$, 1H, He), 2.34 (t, $J = 6.8$, 1H, Hd), 2.36–2.41 (m, 2H, Hb), 3.00–3.12 (m, 2H, Ha), 3.47–3.51 (m, 1H, Hc), 7.21 (dd, $J = 4.8$, 8.4, 1H, PyH), 8.13 (ddd, $J = 1.6$, 2, 8.4, 1H, PyH), 8.25 (dd, $J = 1.6$, 4.8, 1H, PyH), 8.33 (br s, 1H, NH), 8.51 (d, $J = 2$, 1H, PyH). ES$^+$-MS: m/z 281[M + H]$^+$. Anal calcd for $C_{13}H_{18}N_2OS_2$: C, 55.28; H, 6.42; N, 9.91. Calcd for $C_{13}H_{18}N_2OS_2 + 0.25$ H_2O: C, 53.57; H, 6.57; N, 9.61. Found: C, 53.24; H, 6.30; N, 8.96. IR (ν (cm^{-1})): 3420 w (NH), 558 w (S—S).

6,8-Dimercaptooctanoic acid pyridin-3-ylamide (2)

Compound **1** (3.83 g, 10 mmol) was dissolved in 50 ml of 1:1 EtOH/water with stirring. $NaBH_4$ (416 mg, 11 mmol) was added and stirred for 60 min or until the solution became colourless. The reaction mixture was diluted with water (100 ml) and extracted with $CHCl_3$ (3 × 75 ml). The combined organic phases were dried over magnesium sulphate ($MgSO_4$), filtered and evaporated to result in a colourless oil. ^{1}H NMR ($CDCl_3$, J (Hz), δ (ppm)): 1.23 (d, $J = 8$, 1H, SH), 1.29 (t, $J = 8$, 1H, SH), 1.40–1.43 (m, 2H, CH_2), 1.44–1.58 (m, 2H, CH_2), 1.58–1.68 (m, 2H, CH_2), 1.81–1.83 (q, $J = 7.6$, 2H), 2.35 (t, $J = 7.6$, 1H), 2.58–2.68 (m, 2H), 2.84 (br m, 1H), 7.21 (dd, $J = 4.8$, 8.4, 1H, PyH), 8.13 (ddd, $J = 1.6$, 2, 8.4, 1H, PyH), 8.25 (dd, $J = 1.6$, 4.8, 1H, PyH), 8.33 (br s, 1H, NH), 8.51 (d, $J = 2$, 1H, PyH). ES$^+$-MS: m/z 283[M + H]$^+$. IR (ν (cm^{-1})): 3420 w (NH), 2536 w (S—H). Anal calcd for $C_{13}H_{20}N_2OS_2$: C, 55.28; H, 6.42; N, 9.91. Calcd for $C_{13}H_{18}N_2OS_2 + 0.5$ H_2O: C, 53.20; H, 7.21; N, 9.54. Found: C, 53.62; H, 6.73; N, 9.37.

Synthesis of gold nanoparticles 3

Sodium naphthalenide was prepared by adding sodium (100 mg) to a dry solution of naphthalene (410 mg) in 35 ml of diglyme. The mixture was degassed and filled with N_2 three times in a Schlenk and then sonicated while under vacuum until dark green solution appeared. $HAuCl_4$ (30 mg, 8.83 × 10^{-5} mol) was dissolved in 20 ml of dry diglyme in a Schlenk to which the sodium naphthalenide reducing solution was added dropwise until the orange gold solution has turned purple. The colloidal suspension was then exposed to air atmosphere to ensure that all the reducing agent is quenched and stirred for 3–4 min. Ligand **1** (0.068 g, 0.17 mmol) was dissolved in 10 ml of diglyme and the resulting solution was added slowly to the reduced gold nanoparticle colloid and stirred for 1 h. The precipitated nanoparticles were then centrifuged and the supernatant decanted. The nanoparticles pellet was washed aided with sonication in ethanol three times to remove any remaining diglyme and **1**. The final pellet was resuspended in 40 ml of methanol aided by gentle sonication for 2–3 min.

The nanoparticles were characterised by TGA that showed a *ca.* 20% mass loss with onset temperature 170°C, occurring gradually over the temperature range 170–400°C indicative of the loss of the organic ligand.

Synthesis of mixed-ligand gold nanoparticles 4

The method of Brust et al. (*26*) was used to prepare tetraalkyl ammonium bromide-protected nanoparticles. $HAuCl_4$ (0.3537 g, 0.95 mmol) was dissolved in 30 ml of H_2O. Trioctyl propyl ammonium bromide (1.9 g, 4.0 mmol) was dissolved in 80 ml of toluene. Both solutions were combined and stirred vigorously for 10 min. A solution of $NaBH_4$ (0.38 g in 25 ml of H_2O) was then added dropwise to the stirred reaction over a period of 30 min ensuring that organic and aqueous phases were mixed together. The resulting deep red colloidal solution was stirred for further 20 min. The organic phase was extracted and washed once with diluted H_2SO_4 (for neutralisation) and five times with distilled water. The organic layer was then dried with Na_2SO_4.

To 20 ml of this tetraalkyl ammonium bromide-protected nanoparticles stock solution was added dodecanethiol solution in acetone (4.62 × 10^{-3} M; 93.6 mg in 100 ml). The reaction mixture was stirred for 2 h. It was then precipitated with methanol, centrifuged and washed several times with methanol and then ether to give dodecanethiol-protected nanoparticles that were then redissolved in chloroform.

Compound **1** (66 mg, 0.24 mmol) was dissolved in 10 ml of chloroform and added to the chloroform solution of the dodecanethiol-protected nanoparticles (20 ml), which contained 20 ml of the original stock solution of the tetraalkyl ammonium bromide-protected nanoparticles (approx. 0.24 mmol of Au). The reaction mixture was stirred for 24 h. The nanoparticles were then precipitated with methanol, centrifuged and washed several times with methanol and then ether. The nanoparticles were then redissolved in chloroform for further study.

Centrifugation experiment

Gold nanoparticles **3** were centrifuged at 11,000 *g* for 2 h and redissolved in absolute ethanol. The concentration was adjusted to the same as that of the methanol colloid by observing the absorption curve. The stock solution (2 ml) was then titrated with 0.216 M solution of tba-Cl in ethanol. After the addition of 0.1 ml of the anion solution, the SPR peak shifted from 532 to 553 nm as it was observed in the methanol colloid of gold. The solution was then placed in a dialysis tubing cellulose membrane (Aldrich, Missouri) of

MW 12,400 cut-off. The tubing was left in a 250 ml beaker of ethanol to dialyse any free tba-Cl out overnight. The absorption spectrum was taken the following day and has shown no change in the resonance peak. To confirm the permeability of the cellulose tubing to tba-Cl in ethanol, a reverse experiment was undertaken in which gold nanoparticles **3** in ethanol were placed in a dialysis tube inside a beaker containing 250 ml of tba-Cl solution (0.216 M). The tube was left overnight and the electronic absorption was recorded the following day. The spectrum exhibited the characteristic drop in absorbance and red shift characteristic of chloride binding by **3**.

Acknowledgements

We thank the EPSRC for a studentship (M.H.F.).

References

(1) Beer, P.D.; Cormode, D.P.; Davis, J.J. *Chem. Commun.* **2004**, 414–415.
(2) Watanabe, S.; Sonobe, M.; Arai, M.; Tazume, Y.; Matsuo, T.; Nakamura, T.; Yoshida, K. *Chem. Commun.* **2002**, 2866–2867.
(3) Astruc, D.; Daniel, M.C.; Ruiz, J. *Chem. Commun.* **2004**, 2637–2649.
(4) Moores, A.; Goettmann, F. *New J. Chem.* **2006**, *30*, 1121–1132.
(5) Turner, D.R.; Smith, B.; Goeta, A.E.; Evans, I.R.; Tocher, D.A.; Howard, J.A.K.; Steed, J.W. *Cryst. Eng. Comm*. **2004**, *6*, 633–641.
(6) Turner, D.R.; Spencer, E.C.; Howard, J.A.K.; Tocher, D.A.; Steed, J.W. *Chem. Commun.* **2004**, 1352–1353.
(7) Turner, D.R.; Smith, B.; Spencer, E.C.; Goeta, A.E.; Evans, I.R.; Tocher, D.A.; Howard, J.A.K.; Steed, J.W. *New J. Chem.* **2005**, *29*, 90–98.
(8) Filby, M.H.; Humphries, T.D.; Turner, D.R.; Kataky, R.; Kruusma, J.; Steed, J.W. *Chem. Commun.* **2006**, 156–158.
(9) Filby, M.H.; Steed, J.W. *Coord. Chem. Rev.* **2006**, *250*, 3200–3218.
(10) Zhang, J.; Bond, A.M.; Belcher, J.; Wallace, K.J.; Steed, J.W. *J. Phys. Chem. B* **2003**, *107*, 5777–5786.
(11) Wallace, K.J.; Belcher, W.J.; Turner, D.R.; Syed, K.F.; Steed, J.W. *J. Am. Chem. Soc.* **2003**, *125*, 9699–9715.
(12) Turner, D.R.; Paterson, M.J.; Steed, J.W. *J. Org. Chem.* **2006**, *71*, 1598–1608.
(13) Belcher, W.J.; Fabre, M.; Farhan, T.; Steed, J.W. *Org. Biomol. Chem.* **2006**, *4*, 781–786.
(14) Russell, J.M.; Parker, A.D.M.; Radosavljevic-Evans, I.; Howard, J.A.K.; Steed, J.W. *Chem. Commun.* **2006**, 269–271.
(15) Steed, J.W. *Chem. Commun.* **2006**, 2637–2649.
(16) Nieto, S.; Pérez, J.; Riera, L.; Riera, V.; Miguel, D. *New J. Chem.* **2006**, *30*, 838–841.
(17) Wallace, K.J.; Daari, R.; Belcher, W.J.; Abouderbala, L.O.; Boutelle, M.G.; Steed, J.W. *J. Organomet. Chem.* **2003**, *666*, 63–74.
(18) Bondy, C.R.; Gale, P.A.; Loeb, S.J. *Chem. Commun.* **2001**, 729–730.
(19) Bondy, C.R.; Gale, P.A.; Loeb, S.J. *J. Am. Chem. Soc.* **2004**, *126*, 5030–5031.
(20) Schulz-Dobrick, M.; Sarathy, K.V.; Jansen, M. *J. Am. Chem. Soc.* **2005**, *127*, 12816–12817.
(21) Batten, S.R.; Hoskins, B.F.; Moubaraki, B.; Murray, K.S.; Robson, R. *Chem. Commun.* **2000**, 1095–1096.
(22) Chechik, V. *J. Am. Chem. Soc.* **2004**, *126*, 7780–7781.
(23) LizMarzan, L.M.; Giersig, M.; Mulvaney, P. *Langmuir* **1996**, *12*, 4329–4335.
(24) Kim, T.; Lee, K.; Gong, M.S.; Joo, S.W. *Langmuir* **2005**, *21*, 9524–9528.
(25) Tilaki, R.M.; Zad, A.I.; Mahdavi, S.M. *J. Nanoparticle Res.* **2007**, *9*, 853–860.
(26) Brust, M.; Walker, M.; Bethell, D.; Schiffrin, D.J.; Whyman, R. *J. Chem. Soc. Chem. Commun.* **1994**, 801–802.
(27) Fink, J.; Kiely, C.J.; Bethell, D.; Schiffrin, D.J. *Chem. Mat.* **1998**, *10*, 922–926.
(28) Hostetler, M.J.; Wingate, J.E.; Zhong, C.J.; Harris, J.E.; Vachet, R.W.; Clark, M.R.; Londono, J.D.; Green, S.J.; Stokes, J.J.; Wignall, G.D.; et al. *Langmuir* **1998**, *14*, 17–30.